Macromolecules

Article

pubs.acs.org/Macromolecules

Precision Synthesis and Distinct Assembly of Double-Chain Giant Surfactant Regioisomers

Xiao-Man Wang,[†] Yu Shao,[†] Jun Xu,[‡] Xin Jin,[†] Rui-Hao Shen,[†] Peng-Fei Jin,[†] Dong-Wei Shen,[†] Jing Wang,[§] Weihua Li,[∥] Jinlin He,*[,‡] Peihong Ni,[‡] and Wen-Bin Zhang*[,†]

[†]Beijing National Laboratory for Molecular Sciences (BNLMS), Key Laboratory of Polymer Chemistry & Physics of Ministry of Education, Center for Soft Matter Science and Engineering, College of Chemistry and Molecular Engineering, Peking University, Beijing 100871, P. R. China

[‡]College of Chemistry, Chemical Engineering and Materials Science, State and Local Joint Engineering Laboratory for Novel Functional Polymeric Materials, Suzhou Key Laboratory of Macromolecular Design and Precision Synthesis, Jiangsu Key Laboratory of Advanced Functional Polymer Design and Application, Soochow University, Suzhou 215123, P. R. China

[§]South China Advanced Institute of Soft Matter Science and Technology, South China University of Science and Technology, Guangzhou 510640, P. R. China

[∥]State Key Laboratory of Molecular Engineering of Polymers, Collaborative Innovation Center of Polymers and Polymer Composite Materials, Department of Macromolecular Science, Fudan University, Shanghai 200433, P. R. China

Supporting Information

ABSTRACT: The delicate influence of minute structural difference, such as regiochemistry, on self-assembly and phase behaviors has been commonly observed in small molecules but rarely in synthetic polymers. Herein, we report the precision synthesis of a series of double-chain giant surfactant regioisomers and their distinct phase structures and phase behaviors. These giant surfactants possess a hydroxyl-functionalized cubic T_8 polyhedral oligomeric silsesquioxane head and two polystyrene tails tethered at *para*-, *meta*-, and *ortho*-configurations and were prepared following the sequential "click" method. As revealed by temperature-dependent small-angle X-ray scattering and bright-field transmission electron microscopy, their order−disorder transition temperatures decrease in the order of *ortho*-, *meta*-, and *para*-isomers, while order−order transitions were observed in the *meta*-isomer from lamellae to double gyroids and in the *ortho*-isomer from double gyroids to hexagonal cylinders upon increasing temperature. The mechanisms are elucidated by the influence of the tethering positions on the different free energy contributions, i.e., the interfacial energy, the head-to-head interaction, and the entropic energy of the tails. The distinct assembly behaviors of the three regioisomers are unusual in macromolecules yet resemble small molecules. It opens an avenue to fine-tune the macromolecular assembly at the level of molecular precision.

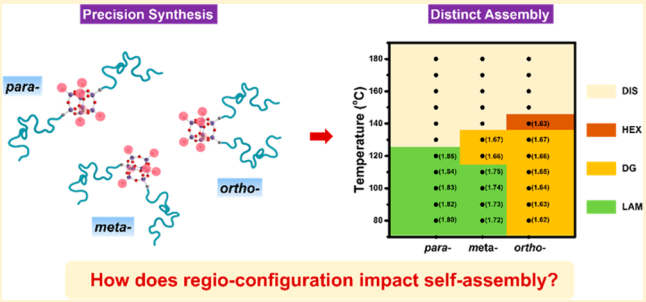

INTRODUCTION

Nature makes extensive use of molecular assembly to produce hierarchically ordered entities with sophisticated structures and functions.[1−3] For decades, people have been trying to mimic this feature in the development of advanced materials. Traditionally, small-molecule surfactants, Janus dendrimers, and block copolymers are among the most versatile artificial self-assembling motifs that exhibit rich self-assembled ordered nanostructures.[4−8] Recently, there emerged a class of "giant molecules" that bridges the gap between small-molecule surfactants and amphiphilic block copolymers, providing new avenues for controlled hierarchical assembly.[9−14] Giant molecules are precise macromolecules constructed using molecular nanoparticles as building blocks. They include giant surfactants, shape amphiphiles, and giant polyhedra. Among them, giant surfactants are size-amplified counterparts of small-molecule surfactants consisting of compact and rigid molecular nanoparticles as the headgroups and flexible polymer chains as the tails.[15] The self-assembly of giant surfactants has been extensively studied both theoretically and experimentally.[16−19] It was found that they possess features reminiscent of both small-molecule surfactants and block copolymers.[20] In solution, they form various micellar morphologies including spheres, wormlike cylinders, and vesicles, in which the polymeric tails are found to be highly stretched, much like that of small-molecule surfactants.[15] In the bulk, they phase-separate into a large variety of ordered nanostructures, including lamellae (LAM), double gyroid (DG), hexagonally

Received: March 8, 2017
Revised: April 27, 2017
Published: May 12, 2017

DOI: 10.1021/acs.macromol.7b00503
Macromolecules 2017, 50, 3943−3953

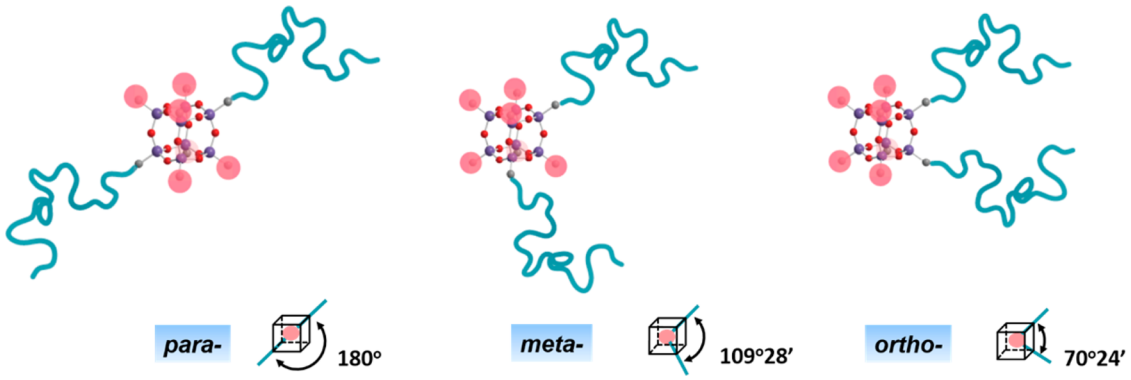

Figure 1. Illustration of double-chain giant surfactant regioisomers with two PS chains (cyan line) and hydroxyl-functionalized POSS head (molecular model with pink side groups). The inset shows the angle between the two tethered chains in these isomers.

Scheme 1. Synthesis of the Double-Chain Giant Surfactant Regioisomers *para-*, *meta-*, and *ortho*-DPOSS-2PS$_n$[a]

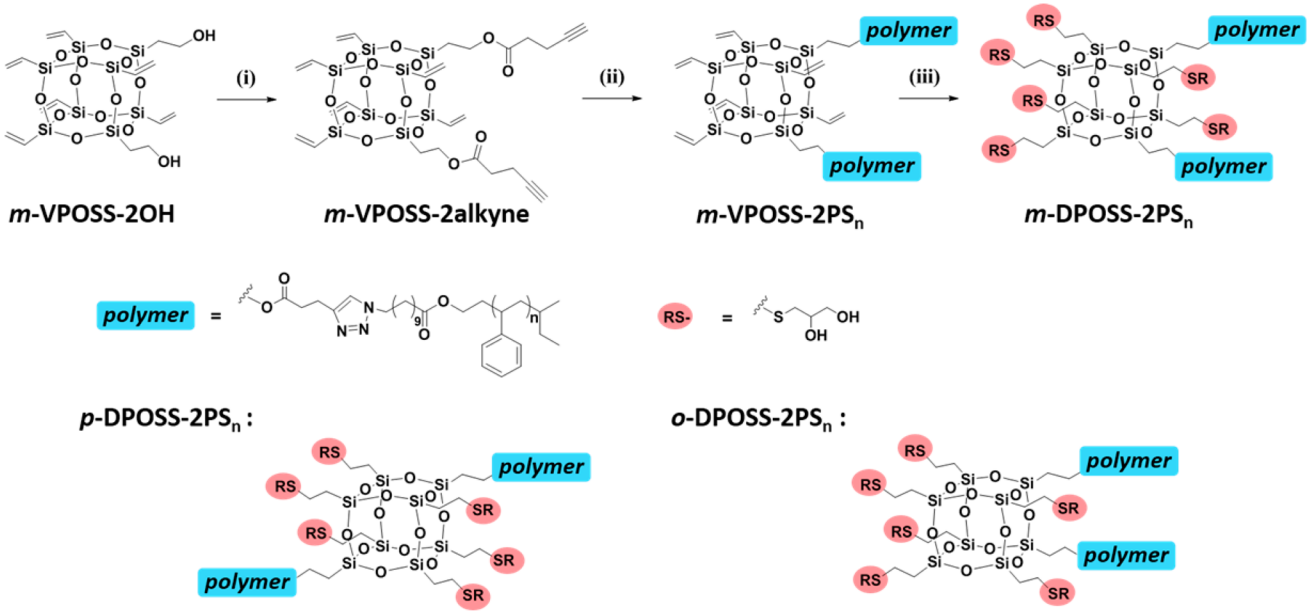

[a]Reagents and conditions: (i) 4-pentynoic acid, DMAP, DIPC, DCM, rt, 12 h, 70−80%; (ii) PS$_n$-N$_3$, CuBr, PMDETA, toluene, rt, 24 h, 68−72%; (iii) 1-thioglycerol, Irgacure 2959, THF, *hv*, 15 min, 70−79%.

packed cylinders (HEX), and body-centered cubic-packed spheres (BCC), much like that of block copolymers.[17,21] The feature sizes of these nanostructures are generally around 10 nm, which is promising for a variety of nanolithographic applications.[22] Although giant molecules are much larger than small molecules in terms of molecular weight and size, their self-assembly exhibits a remarkable sensitivity on the primary chemical structures, and the ability to precisely control their structures affords a versatile platform to explore their self-assembly behaviors with molecular precision.[23]

It has been established that the controlled molecular heterogeneity constitutes the major cause for the formation of unconventional morphologies in macromolecular assemblies,[24] as revealed by the observation of highly concentric lamellae[25] and unusual Frank−Kasper phases[17] formed in giant molecules. Considering the virtually limitless possibilities in the chemical modification of giant surfactants, the full potential of giant surfactants remains to be unleashed to create novel structures and achieve unique properties. To do so, precision synthesis of giant surfactants with complex architectures is a prerequisite, especially of those regio- or stereoisomers, for illustrating the delicate structure−property relationship. Controlling regio- and stereochemistry has been an important subject in polymer chemistry, which was ranked one of the four challenges in polymer chemistry besides sequence, molecular weight, and topology.[26] It often refers to regio- or stereoregularity of the monomers in the polymer chain as in the examples of *isotactic*, *syndio-tactic*, or *atactic* polymers. Such regularity does generate a cumulative, cooperative, and collective effect, leading to dramatic difference on macroscopic properties including crystallinity, glass transition temperature, etc. However, when we consider the difference of only one regio-/stereocenter in the polymer chain, the effect is often insignificant. By contrast, small-molecule self-assemblies are extremely sensitive to such structural variations: adding or removing a methyl group or changing the chirality of one molecule would sometimes completely alter the structures and properties of the assembly.[27,28] It is thus intriguing how the difference in as few as one regiochemistry would impact the self-assembly of giant surfactant isomers. By analogy to small-

DOI: 10.1021/acs.macromol.7b00503
Macromolecules 2017, 50, 3943−3953

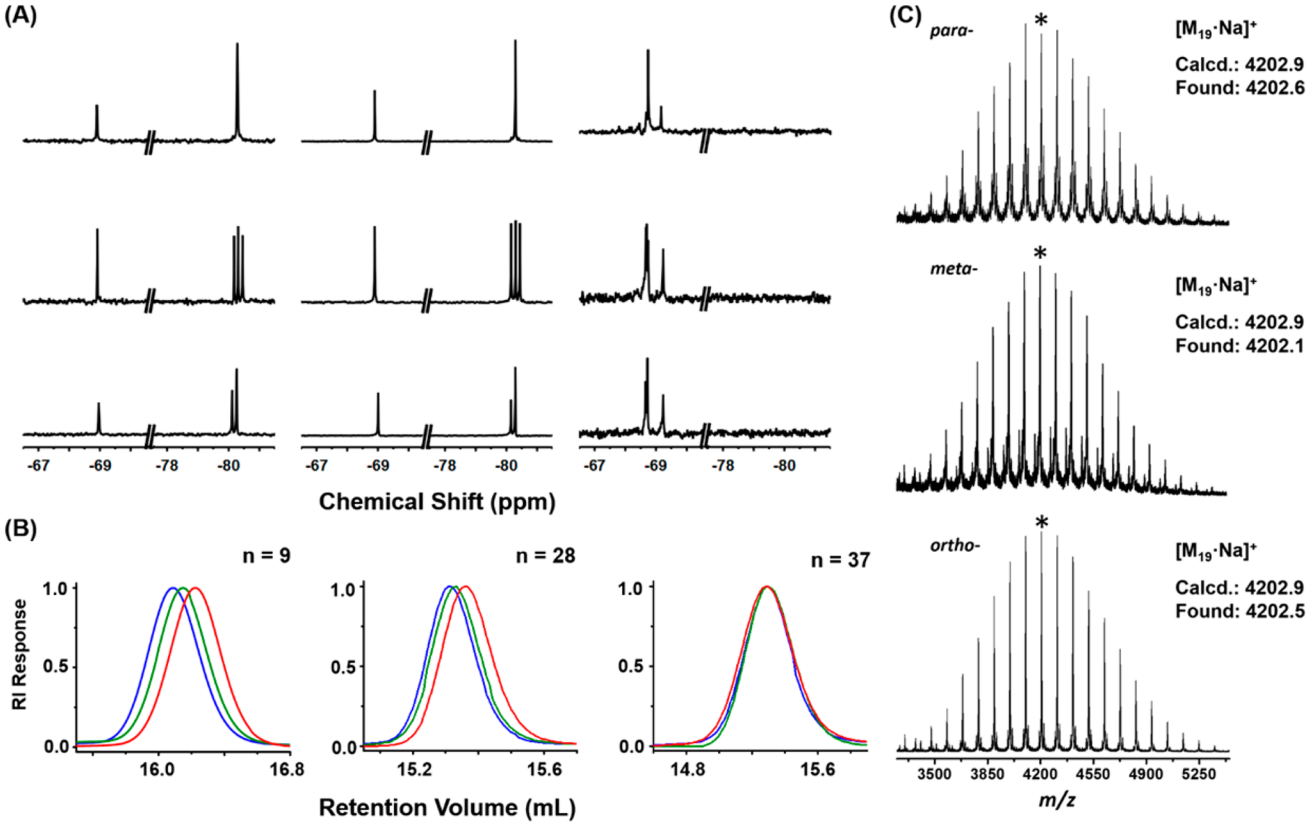

Figure 2. (A) ^{29}Si NMR spectra of VPOSS-2alkyne (left), VPOSS-2PS$_9$ (middle), and DPOSS-2PS$_9$ (right). From top to bottom are *para-*, *meta-*, and *ortho*-isomers, respectively. (B) Overlay of SEC profiles for various sets of VPOSS-2PS$_n$ regioisomers with different n (shown on top). The blue, green, and red curves are *para-*, *meta-*, and *ortho*-isomers, respectively. (C) MALDI-TOF mass spectra for *p*-DPOSS-2PS$_9$ (top), *m*-DPOSS-2PS$_9$ (middle), and *o*-DPOSS-2PS$_9$ (bottom). They almost overlap with each other, suggesting identical MWs and MWDs. The calculated and experimental MWs corresponding to the peaks denoted with asterisks are shown in the inset.

molecule analogues, giant surfactants may contain gemini surfactants, double-chain surfactants, bola-form surfactants, and multiheaded/tailed surfactants.[17,29,30] For double-chain giant surfactants, the location of tails on the surface of molecular nanoparticle head can be varied systematically to create giant surfactant regioisomers. We envision that the relative location of two tails affects the intrinsic interface curvature of the assemblies and thus may have a significant effect on the self-assembly behaviors. To prove this, we must first prepare regioisomers of such giant surfactants.

To date, it remains a big challenge to control the locations of multiple tethering sites on a molecular nanoparticle. Although regiospecific functionalization methods have been developed for polyoxometalates,[31] [60]fullerene,[32] and more recently for POSS,[33−35] it is still difficult to obtain a complete set of giant-molecule regioisomers. Taking advantage of the tiny difference in polarity among different isomers, we were able to obtain a full set of diadduct and triadduct regioisomers based on the cubic T$_8$-POSS nanobuilding blocks with highly reactive vinyl groups and 2-hydroxylethyl groups at the vertexes.[35,36] The *para-*, *meta-*, and *ortho*-isomers can be isolated in synthetically useful quantities, serving as the rigid structural scaffold for various macromolecular architectures including the mixed [2:6] heteroarm star polymers of T$_8$PS$_6$PCL$_2$ via a combination of "growing-from" and "grafting-to" methods.[37] To prepare regioisomers with strictly the same molecular parameters, including molecular weights and polydispersity, it is better to use the "grafting-to" method aided by "click" chemistry.[38,39] In this article, we report the first precision synthesis of a complete series of *para-*, *meta-*, and *ortho-* double-chain giant surfactant regioisomers (Figure 1), their full molecular characterizations, and the distinct self-assembly behaviors for one set of regioisomers. Our results indicate that the sole change of the regioconfiguration is already sufficient to dramatically alter the phase behaviors of these regioisomers.

RESULTS AND DISCUSSION

Molecular Design and Precision Synthesis. To precisely control the tethering sites of two PS tails on POSS, it is best to start from a precise nanobuilding block with predetermined functional groups of orthogonal reactivities. Recently, we have reported a complete series of Janus T$_8$-POSS regioisomers that are hydroxyl-functionalized vinylPOSS (*p-*, *m-*, and *o*-VPOSS-2OH).[35,36] These diadduct isomers possess three-dimensionally (3D) rigid scaffold with precisely arranged vinyl groups and hydroxyl groups, which makes them ideal nanobuilding blocks for double-chain regioisomeric giant surfactants. The general synthetic route is shown in Scheme 1, which follows the sequential "click" approach.[40−42] The Steglich esterification first installed alkyne "click" functionalities to hydroxyls to afford VPOSS-2alkyne isomers in good yields. The following CuAAC "click" reaction with azide-functionalized polystyrene (PS$_n$-N$_3$) of different molecular weights gave a series of VPOSS-2PS$_n$, where n stands for the degree of polymerization for PS. To achieve high structural uniformity, the PS samples were all prepared first by anionic polymerization, end-capped with ethylene oxide to give chain-end hydroxyl functionality (PS$_n$-

DOI: 10.1021/acs.macromol.7b00503
Macromolecules 2017, 50, 3943−3953

Table 1. Molecular Characterization of the Regioisomers

sample[a]	n[b]	$M_{n,PS}$[c] (kg/mol)	$M_{n,NMR}$[d] (kg/mol)	$M_{n,SEC}$ (kg/mol)[e]	$Đ$[f]	f_{PS}[g]	T_g[h]	T_d[i]
p-VPOSS-2PS$_9$	9	1.2	4.0	4.7	1.04		40.3	315.4
p-DPOSS-2PS$_9$	9	1.2	4.0	4.9	1.06	0.69	42.2	193.1
p-VPOSS-2PS$_{28}$	28	3.2	8.0	9.4	1.06		73.3	317.5
p-DPOSS-2PS$_{28}$	28	3.2	8.0	9.8	1.06	0.86	74.8	200.5
p-VPOSS-2PS$_{37}$	37	4.1	9.8	11.1	1.04		80.9	321.7
p-DPOSS-2PS$_{37}$	37	4.1	9.8	11.8	1.04	0.89	82.4	190.3
m-VPOSS-2PS$_9$	9	1.2	4.0	4.4	1.05		38.5	325.0
m-DPOSS-2PS$_9$	9	1.2	4.0	4.9	1.04	0.69	40.2	189.4
m-VPOSS-2PS$_{28}$	28	3.2	8.0	9.2	1.04		72.2	302.8
m-DPOSS-2PS$_{28}$	28	3.2	8.0	9.8	1.03	0.86	74.7	198.5
m-VPOSS-2PS$_{37}$	37	4.1	9.8	10.6	1.05		80.2	288.2
m-DPOSS-2PS$_{37}$	37	4.1	9.8	11.6	1.05	0.89	82.0	200.1
o-VPOSS-2PS$_9$	9	1.2	4.0	4.0	1.03		39.9	298.2
o-DPOSS-2PS$_9$	9	1.2	4.0	4.7	1.06	0.69	40.7	209.7
o-VPOSS-2PS$_{28}$	28	3.2	8.0	8.3	1.03		72.2	295.4
o-DPOSS-2PS$_{28}$	28	3.2	8.0	9.2	1.03	0.86	74.6	202.2
o-VPOSS-2PS$_{37}$	37	4.1	9.8	11.0	1.03		80.0	302.5
o-DPOSS-2PS$_{37}$	37	4.1	9.8	11.5	1.05	0.89	82.4	205.5

[a]Sample label, the subscripts represent the degree of polymerization. [b]Degree of polymerization for the PS tails, which was calculated based on ^{1}H NMR of PS$_n$-N$_3$. [c]Number-average molecular weights of one PS tail including initiator and linker group, kg/mol, as measured by ^{1}H NMR. [d]Number-average molecular weights of DPOSS-2PS$_n$, kg/mol, as measured by ^{1}H NMR. [e]Number-average molecular weights, kg/mol, as measured by SEC. [f]Polydispersity index, as measured by SEC. [g]Volume fraction of PS for DPOSS-2PS$_n$. [h]Glass transition temperature, as measured by DSC with a heating rate of 20 °C/min. [i]Decomposition onset temperature as measured by TGA with a heating rate of 10 °C/min.

OH), esterified with 11-bromoundecanoic acid, and then converted to PS$_n$-N$_3$ by reaction with sodium azide (Scheme S1). The structure of PS$_n$-N$_3$ was confirmed by ^{1}H and ^{13}C NMR spectra, and the degree of azido functionalization was found to be almost quantitative (Figure S1). The VPOSS-2PS$_n$ were modified with 1-thioglycerol using thiol−ene "click" chemistry to impart the amphiphilic feature and give DPOSS-2PS$_n$, where DPOSS represents the hydroxyl-functionalized POSS head. The yields are generally 70% or higher for each step. It is important to note that the head functionalities could also be varied to be hydrophobic, fluorophilic, etc., giving rise to various giant surfactants.[23,43]

The molecular characterizations confirmed the covalent bonding of VPOSS to the polymer chain and more importantly the topological differences of these regioisomers. First, the "clickable" precursor VPOSS-2alkyne as a white powder has been carefully characterized by ^{1}H NMR (Figure S2), ^{13}C NMR (Figure S3), and MALDI-TOF mass spectrometry (Figure S4). For all VPOSS-2alkyne samples, the introduction of two alkyne groups is evidenced by the appearance of a new peak at 1.96 ppm which is the characteristic peak of alkyne proton, and the methylene proton near oxygen has a clearly upfield from ∼3.80 to ∼4.25 ppm in ^{1}H NMR spectra (Figure S2) and two new peaks at ∼82.5 and ∼69.0 ppm in the ^{13}C NMR spectra (Figure S3) which can be assigned as sp carbons in alkyne groups. The differences between the isomers are seen both in the vinyl proton resonance patterns (Figure S5) and in the ^{29}Si NMR spectral patterns (Figure 2A), which remain unchanged during chemical transformations.

The progress of sequential "click" reactions was followed by ^{1}H NMR (Figure S6), ^{13}C NMR (Figure S7), and FT-IR spectra (Figure S8). After the CuAAC "click" reaction, the resonance of the methylene protons near the alkyne shifts completely from 2.51 ppm (*f* in Figure S6A) to 3.03 ppm (*j* in Figure S6B), suggesting successful and clean ligation. More importantly, the characteristic spectral pattern of vinyl protons for each adduct remains largely unchanged compared with the VPOSS-2OH precursors except for some minor changes in chemical shifts (Figure S5), which again indicates that the configuration of the precursor is preserved. The exemplary MALDI-TOF mass spectra of VPOSS-2PS$_9$ (Figure S9) shows only one clean distribution with expected MWs, confirming again the precise structure. After thiol−ene "click" modification, the vinyl proton resonances at 6.15−5.85 ppm completely disappear, and there emerge the thiol−ether methylene resonances around 2.73 ppm (Figure S6C). The molecular weights can be calculated based on ^{1}H NMR spectra, and the results are shown in Table 1. The trend is similar in the ^{29}Si NMR spectra (Figure 2A and Table S1). Upon esterification, there is only a very small upfield shift for Si attached to sp^3 carbon and downfield shift for Si atom attached to vinyl groups.[44] After ligation with PS tails, the chemical shifts and patterns of the Si atoms in VPOSS-2PS$_n$ are almost identical to the corresponding precursors, which indicates that remote functionalization of alkyne with polystyrene have little influence on the chemical environments of POSS core. The thiol−ene reaction converts sp^2 vinyl carbons to sp^3 carbons, leading to a dramatic change in the chemical shift of corresponding Si atom to ∼−69 ppm. Although the resolution is not as good as in previous samples, one can still clearly distinguish the non-equivalent Si atoms attached to thiol−ethers and assign them accordingly (Figure S10).[36] This is a clear evidence that these regioisomers possess distinct configuration.

The distinct configuration also has a direct influence on their elution profiles in SEC (Figure 2B and Figure S11). There is a consistent trend for all of the regioisomers that *para*-isomer has the shortest retention time followed by the *meta*-isomer and the *ortho*-isomer elutes the last. It suggests that the *para*-isomer probably adopts the most expanded conformation, and the hydrodynamic radius is thus the largest; the *ortho*-isomer is the most compact one owing to the closely crowded polymer chains; and the *meta*-isomer is somewhere in between. The

DOI: 10.1021/acs.macromol.7b00503
Macromolecules 2017, 50, 3943−3953

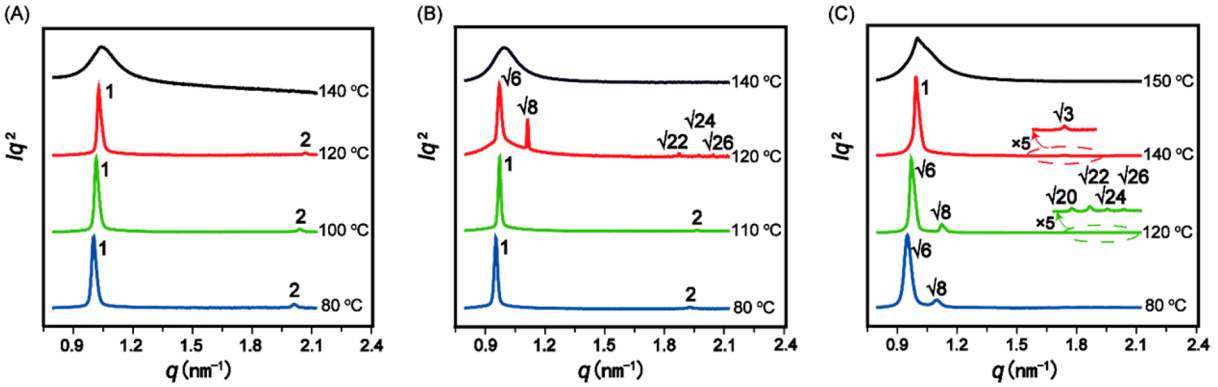

Figure 3. Temperature-dependent SAXS profiles of *p*-DPOSS-2PS$_9$ (A), *m*-DPOSS-2PS$_9$ (B), and *o*-DPOSS-2PS$_9$ (C).

Table 2. Phase Structure Characterizations of DPOSS-2PS$_9$ Regioisomers

samples	f_{PS}[a]	T[b] (°C)	phase structure	q_1[c] (nm^{-1})	d[d] (nm)	a[d] (nm)	A_0[e] (nm^2)
p-DPOSS-2PS$_9$	0.69	80	LAM	0.998	6.28	6.28	1.80
m-DPOSS-2PS$_9$	0.69	80	LAM	0.953	6.59	6.59	1.72
o-DPOSS-2PS$_9$	0.69	80	DG	0.952	6.60	16.17	1.62
m-DPOSS-2PS$_9$	0.69	120	DG	0.972	6.46	15.82	1.66
o-DPOSS-2PS$_9$	0.69	120	DG	0.971	6.47	15.85	1.66
o-DPOSS-2PS$_9$	0.69	140	HEX	0.994	6.32	7.30	1.63

[a]Volume fraction of PS for DPOSS-2PS$_9$. [b]Temperature at which the phase was developed and the SAXS experiments were performed. [c]Data obtained from SAXS profile collected in situ at specific temperature T. [d]Data calculated from q_1. [e]Average interfacial area per molecule; the detailed calculations can be found in the Supporting Information.

result is consistent with the conclusion from the two-dimensional TWIM MS experiment and computer simulation on VPOSS-(S-BPOSS)$_2$ in a previous study[45] that the *para-*, *meta-*, and *ortho*-isomers have different sizes in the order of *para-* > *meta-* > *ortho-*. The difference is the most remarkable for VPOSS-2PS$_n$ with the lowest MW PS tails. As n increases, the geometry of the POSS molecule relative to the whole size of the regioisomers decreases, and thus the size difference between the three regioisomers tapers off and eventually becomes indiscernible. Interestingly, for DPOSS-2PS$_n$ samples, the effect is not as significant (Figure S11). We speculated that the DPOSS head with multiple hydroxyls tends to interact more with the THF solvent, mostly through hydrogen bonding, leading to generally larger hydrodynamic volumes as evidenced by their smaller retention volumes in SEC. The differences among them thus become only marginal. The precisely defined isomeric structure with identical MWs is also unambiguously confirmed by the MALDI-TOF mass spectra. Not only are the observed monoisotopic mass values for each peak in excellent agreement with the calculated ones for all three samples, but also their overall distribution and polydispersity are very much the same from a parallel comparison of the exemplary DPOSS-2PS$_9$ samples (Figure 2C). Therefore, this set of precisely defined DPOSS-2PS$_n$ regioisomers possesses identical MWs and polydispersity but distinct regioconfiguration. They serve as ideal models to illustrate the effect of regioconfiguration on their self-assembly behaviors.

Phase Structures and Phase Transition Behaviors in the Bulk. To illustrate the effects of regioconfiguration on phase structures and phase transition behaviors of these double-chain giant surfactants, we focused on the set of regioisomers with low MW PS tails: *p-*, *m-*, and *o*-DPOSS-2PS$_9$. To choose appropriate temperatures for thermal treatment, the samples were first characterized by thermal gravimetric analysis (TGA) and differential scanning calorimetry (DSC) (Table 1). Their decomposition onset temperatures (T_d), as shown by TGA, are generally higher than 190 °C (Figure S12). The DSC thermal diagrams (Figure S13) reveal the values of T_g of the PS blocks which are consistently higher in DPOSS-2PS$_n$ than that in VPOSS-2PS$_n$ by ∼1−2 °C. This difference should result from the phase separation between PS tails and DPOSS, which makes the PS chains more closely packed. Before thermal annealing, the samples were first heated to above their disorder temperatures (∼180 °C) to eliminate thermal history and remove any effects from residual solvents. The samples were then quenched to specific temperatures for isothermal annealing to develop the thermodynamically equilibrium phase structures. The annealing temperature (T_{anneal}) is chosen to be higher than the corresponding T_gs for favorable relaxation kinetics but lower than T_d to avoid any decomposition. Owing to the lack of chain entanglement in these short PS tails, the phase-separation kinetics is sufficiently fast even at a temperature as low as 80 °C. At 80 °C, both *p-* and *m*-DPOSS-2PS$_9$ assemble into the lamellae (LAM) phase, as indicated by the q ratio of 1:2 in the small-angle X-ray scattering (SAXS) profile, yet with slightly different layer d-spacing (Figure 3A,B). By contrast, *o*-DPOSS-2PS$_9$ forms a double gyroid (DG) phase at 80 °C, as demonstrated by the q ratio of $\sqrt{6}$:$\sqrt{8}$ in the SAXS pattern (Figure 3C).

Temperature-dependent SAXS experiments were then performed at 10 °C interval from 80 to 180 °C to explore their phase transition sequences (Figure 3 and Figures S14−S16). For the *p*-DPOSS-2PS$_9$, the LAM phase is observed as the only ordered phase, and it transfers to the disordered phase (DIS) at 130 °C. In contrast, LAM is also observed in the *m*-DPOSS-2PS$_9$ sample at lower temperatures, and there is an order−order transition (OOT) from LAM to DG at 120 °C. Consequently, the order−disorder transition (ODT) occurs

DOI: 10.1021/acs.macromol.7b00503
Macromolecules 2017, 50, 3943−3953

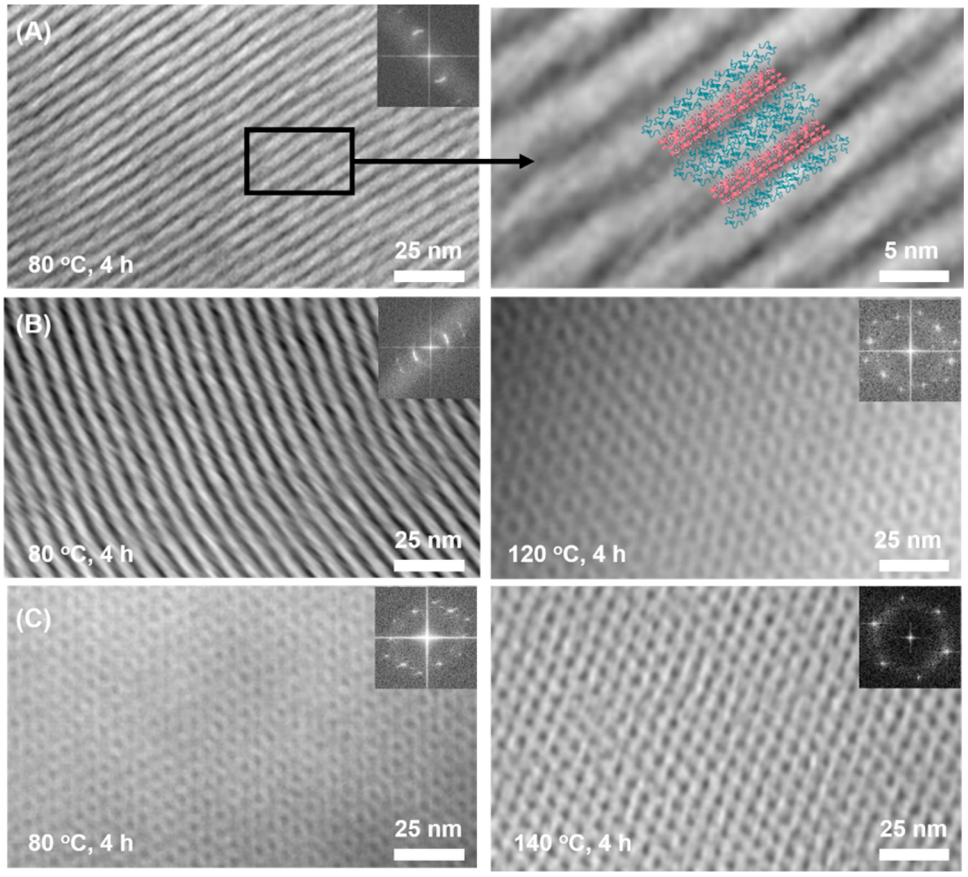

Figure 4. TEM images of the microtomed samples of DPOSS-2PS$_9$ developed at different temperatures: (A) *para*-isomer at 80 °C, LAM phase (left), the zoom-in view and the molecular packing model (right); (B) *meta*-isomer at 80 °C, LAM phase (left), and at 120 °C, DG phase (right); (C) *ortho*-isomer at 80 °C, DG phase (left), and at 140 °C, HEX phase (right). The insets are the corresponding diffraction patterns obtained from fast Fourier transformation of the images.

between the DG and DIS at a temperature around 140 °C, which is noticeable higher than the ODT of the *p*-DPOSS-2PS$_9$ sample. Apparently, the difference of the phase transitions between the *p*- and *m*-DPOSS-2PS$_9$ implies a shift of phase boundaries toward the direction of asymmetric composition and higher interfacial curvature. This tendency continues when the *meta*-configuration is changed further to the *ortho*-one, leading to the presence of another ordered HEX phase at higher temperatures and an even higher ODT at ∼150 °C in the *ortho*-isomer. The HEX phase is usually formed in the region of more asymmetric composition than DG. The ODT is identified from both a sharp decrease of the scattering peak intensity (Figure S17) and a sudden increase of full width at half-maximum (FWHM) of the primary peak (Figure S18). It is important to note that these order−order transitions (OOTs) and order−disorder transitions (ODTs) are fully reversible.

It is anticipated that not only phase transitions but also the domain spacing of the ordered phases would both be influenced considerably by the regioconfiguration. The feature size (a) referres to the layer spacing of LAM, the cubic dimension of DG, and the intercolumnar distance of HEX. It can be estimated based on the primary d-spacing (d) from the corresponding first diffraction peak (q_1) in the SAXS pattern (see Table 2 and Table S2). It is observed that d decreases almost linearly with increasing temperature for each ordered phase formed in a specific sample (Figures S14−S16 and S19). A similar tendency has been commonly observed in many self-assembly systems, such as giant surfactants with a fluorous headgroup,[23] amphiphilic liquid crystals,[46] and block copolymers.[47,48] There exists a fundamental methanism that increasing temperature raises the contribution of the configurational entropy relative to the interfacial energy and therefore reduces the stretching of the PS tails.

To further confirm the ordered morphologies in real space, the samples with the same thermal history as in the SAXS experiments were prepared, quenched in liquid nitrogen to fix the phase morphology, microtomed at room temperature, and then stained with OsO_4 for TEM observations. Typical bright-field TEM micrographs are shown in Figure 4 along with their optical diffraction patterns obtained from fast Fourier transformation. The DPOSS heads and the PS tails are expected to be in the dark and bright/gray domains, respectively. The patterns as well as their feature sizes agree well with the results from SAXS experiments. For example, the layer spacings for LAM of *p*- and *m*-DPOSS-2PS$_9$ is measured to be 6.2 ± 0.5 and 6.6 ± 0.5 nm, respectively, which matches the values of 6.28 and 6.59 nm determined from SAXS experiments (Table S2). The domain sizes for PS (d_{PS}) and for DPOSS (d_{DPOSS}) can be measured from the gray and dark area in the TEM micrograph. In the LAM, these values can also be estimated simply based on the layer spacing d and the volume fraction assuming a sharp interface. Alternatively, the values can be obtained by correlation length analysis of the SAXS data according to Porod's law and the following cosine transformation (Figure S20).[49−52] These thickness parameters can be compared and are crucial for understanding their molecular packing in the self-

DOI: 10.1021/acs.macromol.7b00503
Macromolecules 2017, 50, 3943−3953

assembled domains (Table S3). With all these identified phases, a phase diagram was then constructed (Figure 5).

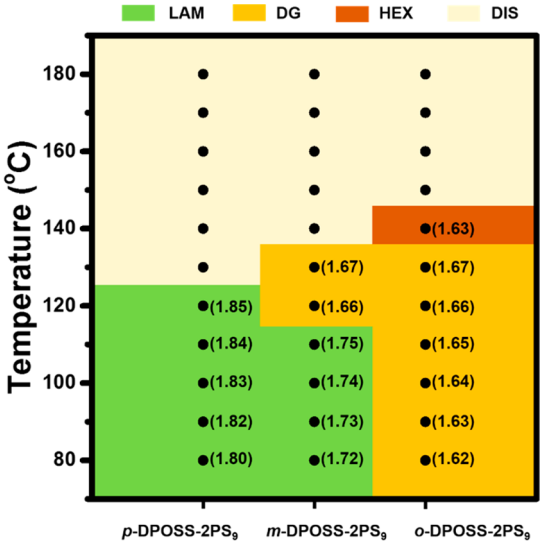

Figure 5. Phase diagram of *p*-DPOSS-2PS$_9$ (left,), *m*-DPOSS-2PS$_9$ (middle), and *o*-DPOSS-2PS$_9$ (right) with respect to temperature. The colors are green for LAM, orange for DG, and brown for HEX. The data in parentheses are the corresponding interfacial area per molecule (A_0) in units of nm^2.

Molecular Packing of Regioisomers in the Ordered Structures. The phase diagram shows that the regioconfiguration of the double-chain giant surfactant isomers does have a remarkable influence on the formation of ordered phases as well as their phase transitions. Intuitively, the main effect of the regioconfiguation is via the molecular packings in the self-assembled domains. Generally speaking, double-chain giant surfactants can adopt three possible configurations: (i) the bridging configuration where the two tails are located at the opposite side of DPOSS; (ii) the partial interdigitation configuration where the two tails are seggregated onto one side of the DPOSS heads and the heads are partially interdigitated (e.g., close-packed); and (iii) the exactly opposing head-to-head and tail-to-tail configuration (Figure 6A). It was found that the values of d_{DPOSS} are generally much larger than the diameter of the DPOSS head (~1.4 nm)[24] but smaller than twice the diameter (~2.8 nm) (Table S3). Therefore, it is reasonable to deduce that both *p*- and *m*-DPOSS-2PS$_9$ primarily adopt the second configuration, the partially interdigitated bilayered molecular packing. It could apparently benefit the maximization of the collective hydrogen bonding among the closely packed heads and the minimization of the interfacial area between DPOSS and PS, especially for the *meta*-isomer. Meanwhile, it also inevitably induces a considerable loss of configurational entropy by enforcing the two tails to extend toward the same side in the *para*-isomer with the largest separation of the tethering points in space. Although the bridging configuration could be advantageous in reducing the entropy loss in the *para*-isomer, the single-layered packing causes an unfavorably high interfacial energy due to a large interface per molecule. Therefore, there may exist a very small portion of bridging configurations in the *para*-isomer as a compromise, which does not disrupt the bilayered molecular packing. This portion is expected to increase as temperature

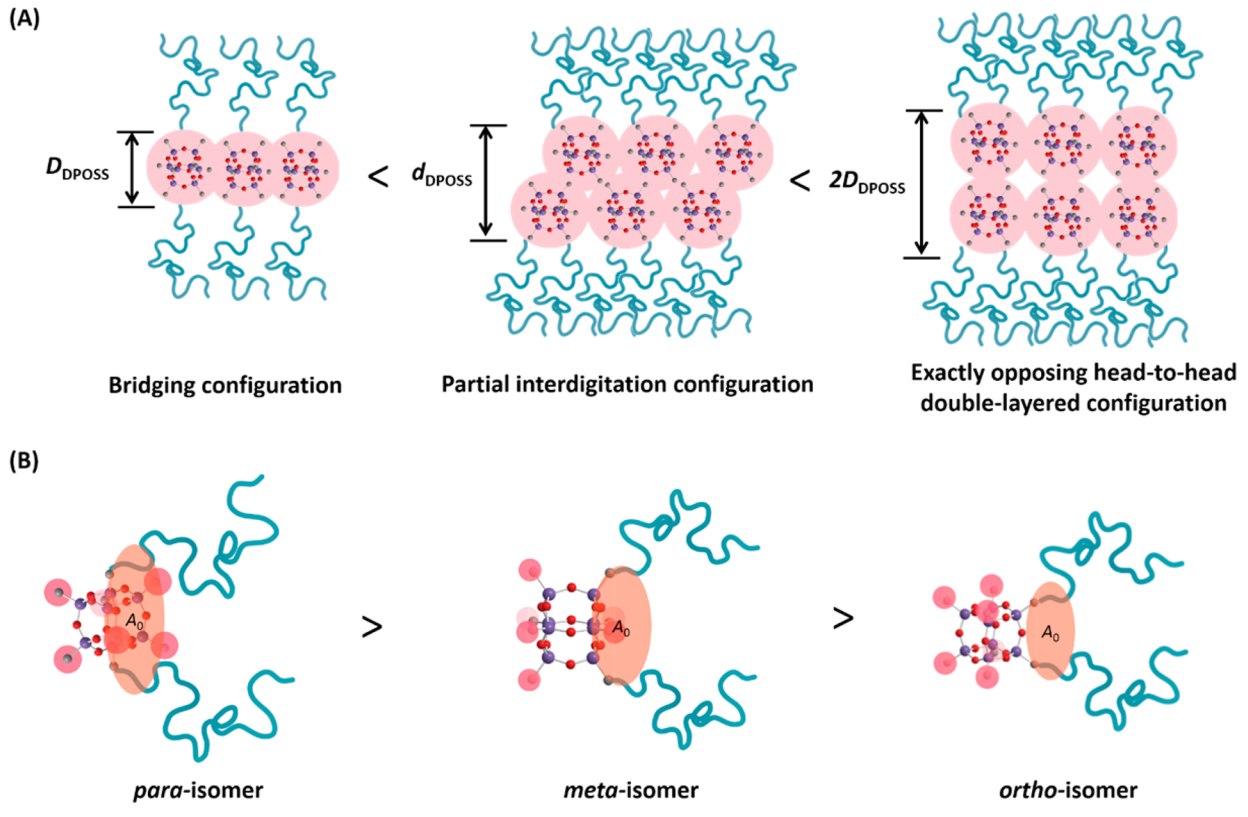

Figure 6. (A) The possible packing schemes for DPOSS-2PS$_9$. (B) The bending of PS tails toward one side in the *para*-isomer leads to a larger interfacial area A_0 as compared to that of *meta*- and *ortho*-isomers.

DOI: 10.1021/acs.macromol.7b00503
Macromolecules 2017, 50, 3943−3953

raises. In contrast, the probability of bridging configuration is apparently low for the *meta*-isomer and quite unlikely for the *ortho*-isomer. The existence of bridging configurations would require the flexible linker between DPOSS and PS, and even part of the PS tails, to penetrate through the DPOSS domains, which reduces the effective volume fraction of PS. In other words, the *para*-isomer possesses the lowest effective volume fraction of PS. This partially contributes to the phase boundary shift toward more asymmetric compositions from the *para*- to *meta*- and *ortho*-isomers in sequence.

To shed light onto the effect of the regioconfiguration on the stability of various ordered phases, we calculated the average cross-sectional area A_0 per molecule and the grafting densities (σ). For LAM phase, it can be calculated using eq 1:

$$A_0 = \frac{2M_{PS}}{a\rho_{PS}N_A f_{PS}} \quad (1)$$

where a is the layer spacing, ρ_{PS} is the density of polystyrene (~1.05 g/cm^3), M_{PS} is the molecular weights of PS, f_{PS} is the volume fraction of PS, and N_A is the Avogadro constant. For DG phase, the A_0 can be estimated according to eq 2:

$$A_0 = \frac{xM_{PS}}{a\rho_{PS}N_A f_{PS}} \quad (2)$$

where a is the unit length of the cubic unit cell and x is the specific surface area to bulk volume ratio of the DG structure as a function of the volume fraction of the gyroid network. This value can be obtained from literature directly.[53] For HEX phase, the A_0 is obtained by eq 3:

$$A_0 = \sqrt{\frac{8\pi f_{DPOSS}}{\sqrt{3}}}\,\frac{M_{PS} + M_{DPOSS}}{a(\rho_{PS}f_{PS} + \rho_{DPOSS}f_{DPOSS})N_A} \quad (3)$$

where a is the intercolumnar distance, ρ_{DPOSS} is the density of POSS head (~1.43 g/cm^3),[24] M_{DPOSS} is the molecular weights of DPOSS (1477 g/mol), and f_{DPOSS} is the volume fraction of DPOSS. If we consider the PS tails as tethered polymer brushes on the interfaces, we can calculated the grafting density (σ) and reduced grafting density ($\tilde{\sigma}$) according to eqs 4 and 5:[54]

$$\sigma = 2/A_0 \quad (4)$$

$$\tilde{\sigma} = 2\pi {R_g}^2/A_0 \quad (5)$$

where R_g is the radius of gyration and represents the unperturbed dimension of the PS tails.[15,29,55] Consequently, we can semiquantitatively evaluate how the conformations of the PS tails deviate from their most probable dimensions by the stretching ratio (S):

$$S = \frac{d_{PS}}{2R_g} \quad (6)$$

where d_{PS} is the PS domain size. The results are summarized in Figure 5, Table 2, and Table S4.

As shown in Figure 5, it is evident that in LAM phase *p*-DPOSS-2PS$_9$ has a larger A_0 value than *m*-DPOSS-2PS$_9$ at the same temperature. This is consistent with the double-layer packing scheme where the two tails in the *para*-isomer have to bend toward the same direction, and thus, the molecule occupies a larger area at the interface. The A_0 value decreases from *para*- to *meta*- and to *ortho*-isomer to favor phases with higher curvature. For all of the samples, the A_0 value increases with increasing temperature but drops to a lower value if an OOT occurs. For *meta*- and *ortho*-isomers, when they exhibit the same phases (DG) at same temperatures, their A_0 values are also identical to each other. Because molecular geometry has tremendous effects on the A_0 values which, in turn, are associated with the free energy of the interface, we believe that it is a critical parameter to understand the effect of regioconfiguration on the assemblies of these isomers.

Effects of Regioconfiguration on the Assemblies. A recent report has shown that by introducing more tails to the DPOSS head, the cross-sectional area of the PS tails increases and higher interfacial curvature toward the DPOSS domain is thus favored, resulting in a phase boundary shift.[17] In current work, while the number of PS tails remains unchanged, varying their tethering positions causes a similar effect to shift phase boundary toward phases with higher interfacial curvatures from *para*- to *meta*- and to *ortho*-isomers at identical f_{PS} and temperature. Considering the two PS tails are pointing to the same side of POSS, the polymer chains are most crowded in the *ortho*-configuration (the smallest A_0 values, Figure 6B), and thus, it would favor the highest interfacial curvature toward the DPOSS domain.

The phase stability can be evaluated based on A_0 and $\tilde{\sigma}$ in a relative scale. As shown in Table S4, the reduced grafting density ($\tilde{\sigma}$) is ~7.0 for the LAM phase. This is between the reported values for the onsets of tethered chain overcrowding (3.7) and the onsets of highly stretched brush regime (14.3).[55] Therefore, the polymer chains are supposed to be stretched. With increasing temperature, the $\tilde{\sigma}$ values decrease and the A_0 values increase. These two factors compete to dictate the phase stability. When geometry allows, an OOT takes place toward a phase with higher curvature with respect to DPOSS domain. In such a way the phase structure not only effectively reduces the A_0 value but also partially releases the PS tail stretching, and therefore the overall free energy of the system decreases. This OOT is critically associated with a χ_{eff} (effective interaction parameter) that is highly temperature dependent, which will be further elaborated in the next section. Meanwhile, the A_0 increases with further increasing temperature, and the interaction parameter χ_{eff} decreases. At a point where the stabilizing interactions from the heads could not compensate for the increase in free energy of the interface, the ODT occurs. Because of geometry, the *para*-isomer has higher A_0 and higher interfacial energy even at lower temperatures. The ODT thus occurs at the lowest temperature among the three isomers. For the *ortho*-isomer, the geometry facilitates the phase separation between the head and tails, forming the most hydrogen bonds between head groups and the least interfacial area. Both factors are beneficial for lowering the overall free energy of the system, leading to higher stability of the assembly and a higher T_{ODT}. The *meta*-isomer lies somewhere in between. The phase transition behaviors of DPOSS-2PS$_9$ can thus be rationalized.

Estimation of χ_{eff} and Its Temperature Dependence. The knowledge on the self-assembly of flexible block copolymers has been well established during the past decades.[56,57] Building an appropriate analogy between the regioisomers and corresponding block copolymer architectures should be instructive to the understanding of their self-assembly behaviors. Fortunately, from the point of view of topology, there exists a nice analogy between the *para*-isomer and ABA triblock copolymer and between the *ortho*-isomer and A$_2$B star copolymers, respectively. According to the self-consistent field calculations, the two copolymers have distinct values of $\chi_{eff}N$ at

DOI: 10.1021/acs.macromol.7b00503
Macromolecules 2017, 50, 3943−3953

ODTs, e.g., ~22.0 for ABA[56] and ~18.0 for A_2B at $f_A = 0.69$.[57] Our observation that the *ortho*-isomer exhibits a higher ODT than the *para*-isomer is consistent with this theoretical prediction. Assuming that the χ_{eff} has an identical relationship with temperature for all three isomers and that the scaling relationship of $\chi_{eff} \sim T^{-1}$ still holds, we can roughly estimate the value of χ_{eff} at ODT to be 0.47 for *p*-DPOSS-2PS_9 and 0.38 for *o*-DPOSS-2PS_9, using the reference volume (ν_0) of 118 Å^3 (which corresponds to an *N* of 47).[58] The estimated χ_{eff} values are comparable to many high χ polymers in the literature such as PTMSS−PLA[59] and PS−P4VP.[60] Moreover, if we assume that χ_{eff} follows the well-known relationship with temperature ($\chi_{eff} = A + B/T$), the value of *B* can be estimated to be ~8 × 10^2 K^{-1}, which is much larger than those of conventional block copolymers.[61] It is reasonable since the χ_{eff} in most conventional block copolymers originates from weak van der Waals interactions whereas in this system it is dictated by the relatively stronger, collective, and cooperative hydrogen bonding among the heads.

CONCLUSIONS

In summary, we have successfully synthesized a series of double-chain regioisomeric giant surfactants. The precise structures and right assignment of configurations were unambiguously proven by combined multiple characterizations, including the ^{1}H NMR, ^{13}C NMR, and ^{29}Si NMR spectroscopy. The isomeric structures are evidenced by the almost identical MALDI-TOF mass spectra of these isomers. The topological difference between different regioisomers is shown in the SEC overlay and the glass transition temperatures. This is the first time that the precision synthesis of *para*-, *meta*-, and *ortho*-double-chain regioisomers has been achieved. We also examined the self-assembly behaviors of the three isomers with exactly the same molecular weights. They exhibit distinct phase structures and phase transition behaviors. The difference is rationalized via the influence of regioconfiguration on the molecular arrangements and the free energy changes. The effective interaction parameters were estimated to be ~0.47 and ~0.38, which are comparable to those high-χ polymers. Moreover, while the current study on assembly is limited to the set of samples with shorter PS chains, preliminary results on other samples with longer PS chains indicate that their assembled structures and phase behaviors are also significantly influenced by their regioconfiguration. The work on constructing a complete phase diagram is underway. Altogether, it suggests that regiochemistry may provide an additional dimension for controlling macromolecular self-assembly and fine-tuning the morphology and phase behaviors at sub-10 nm scales.

ASSOCIATED CONTENT

Supporting Information

The Supporting Information is available free of charge on the ACS Publications website at DOI: 10.1021/acs.macromol.7b00503.

Experimental procedures, ^{1}H NMR, ^{13}C NMR, and ^{29}Si NMR spectra, MALDI-TOF mass spectra, SEC traces, calculation details, SAXS data, and additional characterization data (PDF)

AUTHOR INFORMATION

Corresponding Authors

*E-mail jlhe@suda.edu.cn (J.H.).
*E-mail wenbin@pku.edu.cn (W.-B.Z.).

ORCID

Weihua Li: 0000-0002-5133-0267
Peihong Ni: 0000-0003-4572-3213
Wen-Bin Zhang: 0000-0002-8746-0792

Author Contributions

X.-M.W. and Y.S. contributed equally to the work.

Notes

The authors declare no competing financial interest.

ACKNOWLEDGMENTS

We are grateful for the financial support from the National Natural Science Foundation of China (Grants 21674003, 91427304, and 21304061), 1000 Plan (Youth), a Project Funded by the Priority Academic Program Development (PAPD) of Jiangsu Higher Education Institutions, and Beijing National Laboratory for Molecular Sciences (20140152). We thank the Beamline 16B for the assistance with the SAXS experiments at the Shanghai Synchrotron Radiation Facility and Beamline 1W2A for the assistance with the SAXS experiments at the Beijing Synchrotron Radiation Facility.

REFERENCES

(1) Lehn, J. M. Toward Self-organization and Complex Matter. *Science* **2002**, *295*, 2400−2403.
(2) Whitesides, G. M.; Grzybowski, B. Self Assembly at All Scales. *Science* **2002**, *295*, 2418−2421.
(3) Sarikaya, M.; Tamerler, C.; Jen, A. K.-Y.; Schulten, K.; Baneyx, F. Molecular Biomimetics: Nanotechnology Through Biology. *Nat. Mater.* **2003**, *2*, 577−585.
(4) Ikkala, O.; Brinke, G. t. Functional Materials Based on Self-Assembly of Polymeric Supramolecules. *Science* **2002**, *295*, 2407−2409.
(5) Holmberg, K. *Surfactants and Polymers in Aqueous Solution*; 2nd ed.; John Wiley & Sons: Chichester, 2003.
(6) Percec, V.; Wilson, D. A.; Leowanawat, P.; Wilson, C. J.; Hughes, A. D.; Kaucher, M. S.; Hammer, D. A.; Levine, D. H.; Kim, A. J.; Bates, F. S.; Davis, K. P.; Lodge, T. P.; Klein, M. L.; DeVane, R. H.; Aqad, E.; Rosen, B. M.; Argintaru, A. O.; Sienkowska, M. J.; Rissanen, K.; Nummelin, S.; Ropponen, J. Self-Assembly of Janus Dendrimers into Uniform Dendrimersomes and Other Complex Architectures. *Science* **2010**, *328*, 1009−1014.
(7) Mai, Y.; Eisenberg, A. Self-Assembly of Block Copolymers. *Chem. Soc. Rev.* **2012**, *41*, 5969−5985.
(8) Rosen, B. M.; Wilson, C. J.; Wilson, D. A.; Peterca, M.; Imam, M. R.; Percec, V. Dendron-Mediated Self-Assembly, Disassembly, and Self-Organization of Complex Systems. *Chem. Rev.* **2009**, *109*, 6275−6540.
(9) Grosberg, A. I. U.; Khokhlov, A. R.; Gennes, P.-G. d. *Giant Molecules: Here, There, and Everywhere*, 2nd ed.; World Scientific: Hackensack, NJ, 2011.
(10) Zhang, W.-B.; Yu, X.; Wang, C.-L.; Sun, H.-J.; Hsieh, I. F.; Li, Y.; Dong, X.-H.; Yue, K.; Van Horn, R.; Cheng, S. Z. D. Molecular Nanoparticles Are Unique Elements for Macromolecular Science: From "Nanoatoms" to Giant Molecules. *Macromolecules* **2014**, *47*, 1221−1239.
(11) Zhang, W.-B.; Wang, X.-M.; Wang, X.-W.; Liu, D.; Han, S.-Y.; Cheng, S. Z. D. Giant Molecules Based on Nano-Atoms. *Prog. Chem.* **2015**, *27*, 1333−1342.
(12) Zhang, W. B.; Chen, E. Q.; Wang, J.; Zhang, W.; Wang, L. G.; Cheng, S. Z. D. Soft Matters from "Nano-Atoms" to "Giant Molecules". *Acta Phys. Sin.* **2016**, *65*, 183601.

DOI: 10.1021/acs.macromol.7b00503
Macromolecules 2017, 50, 3943−3953

(13) Zhang, W.-B.; Wu, X.-L.; Yin, G.-Z.; Shao, Y.; Cheng, S. Z. D. From Protein Domains to Molecular Nanoparticles: What Can Giant Molecules Learn from Proteins? *Mater. Horiz.* **2017**, *4*, 117−132.
(14) Yin, G. Z.; Zhang, W. B.; Cheng, S. Z. D. Giant molecules: where chemistry, physics, and bio-science meet. *Sci. China: Chem.* **2017**, *60*, 338−352.
(15) Yu, X.; Zhong, S.; Li, X.; Tu, Y.; Yang, S.; Van Horn, R. M.; Ni, C.; Pochan, D. J.; Quirk, R. P.; Wesdemiotis, C.; Zhang, W.-B.; Cheng, S. Z. D. A Giant Surfactant of Polystyrene-(Carboxylic Acid-Functionalized Polyhedral Oligomeric Silsesquioxane) Amphiphile with Highly Stretched Polystyrene Tails in Micellar Assemblies. *J. Am. Chem. Soc.* **2010**, *132*, 16741−16744.
(16) Zhang, T.; Fu, C.; Yang, Y.; Qiu, F. Extremely Asymmetric Phase Diagram of Homopolymer-Monotethered Nanoparticles: Competition Between Chain Conformational Entropy and Particle Steric Interaction. *J. Chem. Phys.* **2017**, *146*, 054902.
(17) Yue, K.; Huang, M.; Marson, R. L.; He, J.; Huang, J.; Zhou, Z.; Wang, J.; Liu, C.; Yan, X.; Wu, K.; Guo, Z.; Liu, H.; Zhang, W.; Ni, P.; Wesdemiotis, C.; Zhang, W. B.; Glotzer, S. C.; Cheng, S. Z. Geometry Induced Sequence of Nanoscale Frank-Kasper and Quasicrystal Mesophases in Giant Surfactants. *Proc. Natl. Acad. Sci. U. S. A.* **2016**, *113*, 14195−14200.
(18) Horsch, M. A.; Zhang, Z.; Glotzer, S. C. Self-Assembly of Laterally-Tethered Nanorods. *Nano Lett.* **2006**, *6*, 2406−2413.
(19) Glotzer, S. C.; Horsch, M. A.; Iacovella, C. R.; Zhang, Z.; Chan, E. R.; Zhang, X. Self-Assembly of Anisotropic Tethered Nanoparticle Shape Amphiphiles. *Curr. Opin. Colloid Interface Sci.* **2005**, *10*, 287−295.
(20) Yu, X.; Li, Y.; Dong, X. H.; Yue, K.; Lin, Z.; Feng, X.; Huang, M.; Zhang, W.-B.; Cheng, S. Z. D. Giant Surfactants Based on Molecular Nanoparticles: Precise Synthesis and Solution Self-assembly. *J. Polym. Sci., Part B: Polym. Phys.* **2014**, *52*, 1309−1326.
(21) Yu, X.; Yue, K.; Hsieh, I.-F.; Li, Y.; Dong, X.-H.; Liu, C.; Xin, Y.; Wang, H.-F.; Shi, A.-C.; Newkome, G. R.; Ho, R.-M.; Chen, E.-Q.; Zhang, W.-B.; Cheng, S. Z. D. Giant Surfactants Provide a Versatile Platform for Sub-10nm Nanostructure Engineering. *Proc. Natl. Acad. Sci. U. S. A.* **2013**, *110*, 10078−10083.
(22) Sinturel, C.; Bates, F. S.; Hillmyer, M. A. High χ−Low N Block Polymers: How Far Can We Go? *ACS Macro Lett.* **2015**, *4*, 1044−1050.
(23) Yue, K.; Liu, C.; Huang, M.; Huang, J.; Zhou, Z.; Wu, K.; Liu, H.; Lin, Z.; Shi, A.-C.; Zhang, W.-B.; Cheng, S. Z. D. Self-Assembled Structures of Giant Surfactants Exhibit a Remarkable Sensitivity on Chemical Compositions and Topologies for Tailoring Sub-10 nm Nanostructures. *Macromolecules* **2017**, *50*, 303−314.
(24) Zhang, W.; Huang, M.; Su, H.; Zhang, S.; Yue, K.; Dong, X.-H.; Li, X.; Liu, H.; Zhang, S.; Wesdemiotis, C.; Lotz, B.; Zhang, W.-B.; Li, Y.; Cheng, S. Z. D. Toward Controlled Hierarchical Heterogeneities in Giant Molecules with Precisely Arranged Nano Building Blocks. *ACS Cent. Sci.* **2016**, *2*, 48−54.
(25) Dong, X. H.; Ni, B.; Huang, M.; Hsu, C. H.; Bai, R.; Zhang, W. B.; Shi, A. C.; Cheng, S. Z. D. Molecular-Curvature-Induced Spontaneous Formation of Curved and Concentric Lamellae through Nucleation. *Angew. Chem., Int. Ed.* **2016**, *55*, 2459−2463.
(26) Odian, G. G. *Principles of Polymerization*; 4th ed.; Wiley-Interscience: Hoboken, NJ, 2004.
(27) Smulders, M. M. J.; Schenning, A. P. H. J.; Meijer, E. W. Insight into the Mechanisms of Cooperative Self-Assembly: The "Sergeants-and-Soldiers" Principle of Chiral and Achiral C_3-Symmetrical Discotic Triamides. *J. Am. Chem. Soc.* **2008**, *130*, 606−611.
(28) Prins, L. J.; Timmerman, P.; Reinhoudt, D. N. Amplification of Chirality: The "Sergeants and Soldiers" Principle Applied to Dynamic Hydrogen-Bonded Assemblies. *J. Am. Chem. Soc.* **2001**, *123*, 10153−10163.
(29) Wang, Z.; Li, Y.; Dong, X.-H.; Yu, X.; Guo, K.; Su, H.; Yue, K.; Wesdemiotis, C.; Cheng, S. Z. D.; Zhang, W.-B. Giant Gemini Surfactants Based on Polystyrene−Hydrophilic Polyhedral Oligomeric Silsesquioxane Shape Amphiphiles: Sequential "Click" Chemistry and Solution Self-Assembly. *Chem. Sci.* **2013**, *4*, 1345−1352.
(30) Yue, K.; Liu, C.; Guo, K.; Wu, K.; Dong, X.-H.; Liu, H.; Huang, M.; Wesdemiotis, C.; Cheng, S. Z. D.; Zhang, W.-B. Exploring Shape Amphiphiles Beyond Giant Aurfactants: Molecular Design and Click Synthesis. *Polym. Chem.* **2013**, *4*, 1056−1067.
(31) Proust, A.; Matt, B.; Villanneau, R.; Guillemot, G.; Gouzerh, P.; Izzet, G. Functionalization and Post-functionalization: A Step towards Polyoxometalate-based Materials. *Chem. Soc. Rev.* **2012**, *41*, 7605−7622.
(32) Hirsch, A.; Brettreich, M. *Fullerenes: Chemistry and Reactions*; Wiley-VCH: Weinheim, 2005.
(33) Oguri, N. E. Y.; Takeda, N.; Unno, M. Janus-Cube Octasilsesquioxane: Facile Synthesis and Structure Elucidation. *Angew. Chem., Int. Ed.* **2016**, *55*, 9336−9336.
(34) Blazquez-Moraleja, A.; Eugenia Perez-Ojeda, M.; Suarez, J. R.; Luisa Jimeno, M.; Chiara, J. L. Efficient Multi-Click Approach to Well-Defined Two-Faced Octasilsesquioxanes: The First Perfect Janus Nanocube. *Chem. Commun.* **2016**, *52*, 5792−5795.
(35) Wang, X.-M.; Guo, Q.-Y.; Han, S.-Y.; Wang, J.-Y.; Han, D.; Fu, Q.; Zhang, W.-B. Stochastic/Controlled Symmetry Breaking of the T8 POSS Cages toward Multifunctional Regio-isomeric Nano-building Blocks. *Chem. - Eur. J.* **2015**, *21*, 15246−15255.
(36) Han, S. Y.; Wang, X. M.; Shao, Y.; Guo, Q. Y.; Li, Y.; Zhang, W. B. Janus POSS Based on Mixed [2:6] Octakis-Adduct Regioisomers. *Chem. - Eur. J.* **2016**, *22*, 6397−6403.
(37) Shao, Y.; Yin, H.; Wang, X.-M.; Han, S.-Y.; Yan, X.; Xu, J.; He, J.; Ni, P.; Zhang, W.-B. Mixed [2:6] Hetero-Arm Star Polymers Based on Janus POSS with Precisely Defined Arm Distribution. *Polym. Chem.* **2016**, *7*, 2381−2388.
(38) Kolb, H. C.; Finn, M. G.; Sharpless, K. B. Click Chemistry: Diverse Chemical Function from a Few Good Reactions. *Angew. Chem., Int. Ed.* **2001**, *40*, 2004−2021.
(39) Iha, R. K.; Wooley, K. L.; Nystrom, A. M.; Burke, D. J.; Kade, M. J.; Hawker, C. J. Applications of Orthogonal "Click" Chemistries in the Synthesis of Functional Soft Materials. *Chem. Rev.* **2009**, *109*, 5620−5686.
(40) Lin, Z.; Lu, P.; Yu, X.; Zhang, W.-B.; Huang, M.; Wu, K.; Guo, K.; Wesdemiotis, C.; Zhu, X.; Zhang, Z.; Yue, K.; Cheng, S. Z. D. Sequential "Click" Synthesis of "Nano-Diamond-Ring-like" Giant Surfactants Based on Functionalized Hydrophilic POSS/C60 Tethered with Cyclic Polystyrenes. *Macromolecules* **2014**, *47*, 4160−4168.
(41) Yue, K.; Liu, C.; Guo, K.; Yu, X.; Huang, M.; Li, Y.; Wesdemiotis, C.; Cheng, S. Z. D.; Zhang, W.-B. Sequential "Click" Approach to Polyhedral Oligomeric Silsesquioxane-Based Shape Amphiphiles. *Macromolecules* **2012**, *45*, 8126−8134.
(42) Su, H.; Zheng, J.; Wang, Z.; Lin, F.; Feng, X.; Dong, X.-H.; Becker, M. L.; Cheng, S. Z. D.; Zhang, W.-B.; Li, Y. Sequential Triple "Click" Approach toward Polyhedral Oligomeric Silsesquioxane-Based Multiheaded and Multitailed Giant Surfactants. *ACS Macro Lett.* **2013**, *2*, 645−650.
(43) Zhang, W.-B.; Li, Y.; Li, X.; Dong, X.; Yu, X.; Wang, C.-L.; Wesdemiotis, C.; Quirk, R. P.; Cheng, S. Z. D. Synthesis of Shape Amphiphiles Based on Functional Polyhedral Oligomeric Silsesquioxane End-Capped Poly(l-Lactide) with Diverse Head Surface Chemistry. *Macromolecules* **2011**, *44*, 2589−2596.
(44) Bassindale, A. R.; Parker, D. J.; Taylor, P. G.; Watt, A. C. Structural Elucidations of T8 and Q8 Silsesquioxane Cages Containing Two Types of Pendant Group Using ^{29}Si NMR Spectroscopy. *Can. J. Chem.* **2003**, *81*, 1341−1349.
(45) Li, Y.; Guo, K.; Su, H.; Li, X.; Feng, X.; Wang, Z.; Zhang, W.; Zhu, S.; Wesdemiotis, C.; Cheng, S. Z. D.; Zhang, W.-B. Tuning "Thiol-Ene" Reactions Toward Controlled Symmetry Breaking in Polyhedral Oligomeric Silsesquioxanes. *Chem. Sci.* **2014**, *5*, 1046−1053.
(46) Jongen, L.; Hinz, D.; Meyer, G.; Binnemans, K. Induced Mesophases in Binary Mixtures of Lanthanide(III) Dodecanoates. *Chem. Mater.* **2001**, *13*, 2243−2246.
(47) Lai, T.-Y.; Cheng, C.-Y.; Cheng, W.-Y.; Lee, K.-M.; Tung, S.-H. Phase Behavior and Structure of Supramolecules Formed by Poly(4-

DOI: 10.1021/acs.macromol.7b00503
Macromolecules 2017, 50, 3943−3953

vinylpyridine) and Fanlike Benzoic Acid Derivative with Long Hydrophobic Tails. *Macromolecules* **2015**, *48*, 717−724.
(48) Ahn, H.; Shin, C.; Lee, B.; Ryu, D. Y. Phase Transitions of Block Copolymer Film on Homopolymer-Grafted Substrate. *Macromolecules* **2010**, *43*, 1958−1963.
(49) Porod, V. G. The X-ray Diffraction Scattering of Densely Packed Colloid Systems. *Colloid Polym. Sci.* **1951**, *124*, 83−114.
(50) Ruland, W. Small-Angle Scattering of Two-Phase Systems: Determination and Significance of Systematic Deviations from Porod's Law. *J. Appl. Crystallogr.* **1971**, *4*, 70−73.
(51) Koberstein, J. T.; Morra, B.; Stein, R. S. The Determination of Diffuse-Boundary. *J. Appl. Crystallogr.* **1980**, *13*, 34−45.
(52) Strobl, G. R.; Schneider, M. Direct Evaluation of the Electron Density Correlation Function of Partially Crystalline Polymers. *J. Polym. Sci., Polym. Phys. Ed.* **1980**, *18*, 1343−1359.
(53) Scherer, M. R. J. *Double-Gyroid-Structured Functional Materials: Synthesis and Applications*; Springer International Publishing: Cham, Switzerland, 2013.
(54) Brittain, W. J.; Minko, S. A Structural Definition of Polymer Brushes. *J. Polym. Sci., Part A: Polym. Chem.* **2007**, *45*, 3505−3512.
(55) Zheng, J. X.; Xiong, H.; Chen, W. Y.; Lee, K.; Van Horn, R. M.; Quirk, R. P.; Lotz, B.; Thomas, E. L.; Shi, A. C.; Cheng, S. Z. D. Onsets of Tethered Chain Overcrowding and Highly Stretched Brush Regime via Crystalline-Amorphous Diblock Copolymers. *Macromolecules* **2006**, *39*, 641−650.
(56) Matsen, M. W. Effect of Architecture on the Phase Behavior of AB-Type Block Copolymer Melts. *Macromolecules* **2012**, *45*, 2161−2165.
(57) Xie, N.; Li, W.; Qiu, F.; Shi, A.-C. σ Phase Formed in Conformationally Asymmetric AB-Type Block Copolymers. *ACS Macro Lett.* **2014**, *3*, 906−910.
(58) Cochran, E. W.; Morse, D. C.; Bates, F. S. Design of ABC Triblock Copolymers near the ODT with the Random Phase Approximation. *Macromolecules* **2003**, *36*, 782−792.
(59) Cushen, J. D.; Bates, C. M.; Rausch, E. L.; Dean, L. M.; Zhou, S. X.; Willson, C. G.; Ellison, C. J. Thin Film Self-Assembly of Poly(trimethylsilylstyrene-b-d,l-lactide) with Sub-10 nm Domains. *Macromolecules* **2012**, *45*, 8722−8728.
(60) Zha, W.; Han, C. D.; Lee, D. H.; Han, S. H.; Kim, J. K.; Kang, J. H.; Park, C. Origin of the Difference in Order-Disorder Transition Temperature between Polystyrene-*block*-poly(2-vinylpyridine) and Polystyrene-*block*-poly(4-vinylpyridine) Copolymers. *Macromolecules* **2007**, *40*, 2109−2119.
(61) Eitouni, H. B.; Balsara, N. P. Thermodynamics of Polymer Blends. In *Physical Properties of Polymers Handbook*, 2nd ed.; Mark, J. E., Ed.; Springer Science Media, LLC: New York, 2007.

DOI: 10.1021/acs.macromol.7b00503
Macromolecules 2017, 50, 3943−3953